Chapter SP   (Seismic Processing)

SEISMIC PROCESSING AND VELOCITY ASSESSMENTS

by Myung W. Lee[1], Warren F. Agena[1], John A. Grow[1], and John J. Miller[1]

in The Oil and Gas Resource Potential of the 1002 Area, Arctic National Wildlife Refuge, Alaska, by ANWR Assessment Team, U. S. Geological Survey Open File Report 98-34.

1999

[1] U.S. Geological Survey, MS 939, Denver, CO 80225

TABLE OF CONTENTS

ABSTRACT
INTRODUCTION
DATA ACQUISITION
DATA PROCESSING
    Demultiplex
    Geometry Definition
    Gain, deconvolution and elevation statics
    Shot-domain F-K filtering
    Velocity analysis and NMO correction
    Residual statics
    Stack
    Shot-domain DMO
    Post-Stack Deconvolution
    Datum Correction and Filtering
    Migration
    Depth Conversion
    Section Enhancement
DERIVATION OF VELOCITIES
    Migration Velocity
    Average Velocity
    Average Velocity to TPM
DISCUSSION
SUMMARY AND CONCLUSION
REFERENCES

TABLES
SP1   Reflection seismic lines on and adjacent to the Arctic National Wildlife
      Refuge
SP2   Parameters of seismic data acquisition in the ANWR area

FIGURES
SP1   Seismic data processing flow chart.
SP2   An example of stacked seismic data showing the effect of pre-stack
      two-dimensional filtering.
SP3   An example of velocity analysis without a dip moveout (DMO)
      correction.
SP4   An example of velocity analysis with a DMO correction.
SP5   An example showing the effect of post-stack deconvolution.

ABSTRACT

Seismic data totaling 1,451 mi (2,351 km) were reprocessed in the Arctic National Wildlife Refuge. All seismic data were stacked, migrated and converted to depth. Most of the seismic profiles except for a few lines in the undeformed area were processed using dip moveout correction to estimate reliable migration and depth conversion velocities. Post-stack wavelet deconvolution was applied to all seismic data in order to increase temporal resolution and to better tie seismic lines acquired with different seismic sources. A three-dimensional velocity model to the top of the Pre-Mississippian was developed using seismically derived velocities and well velocities adjacent to the study area.

INTRODUCTION

In 1984 and 1985, Geophysical Service Inc. (GSI), under contract to a consortium of petroleum exploration companies, acquired and processed 1,451 mi (2,351 km) of multichannel seismic data on and adjacent to the Arctic National Wildlife Refuge (ANWR) as part of a petroleum resource evaluation study. The resource evaluation was performed in 1987 by the Fish and Wildlife Service (FWS), the Bureau of Land Management (BLM) and the U. S. Geological Survey (USGS) (Bird and Magoon, 1987).

During the 1987 resource assessment, the USGS reprocessed about 21% (500.69 km, 311.13 mi) of seismic data in order to prepare the illustrations in the 1987 publication (Bird and Lagoon, 1987) and in the report to Congress (Clough and others, 1987). At that time, the reprocessing was performed on a VAX 11/780 computer using the DIGICON, Inc., DISCO software package and stacked sections were provided for use as illustrations. Details of the reprocessing effort can be found in Leinbach and others (1987).

Recent renewed interest in the amount of petroleum that might exist beneath the coastal plain of the ANWR has resulted in numerous inquiries from Congress, Department of the Interior and various private sectors. As part of the re-evaluation of resource potential in the ANWR, reprocessing of seismic data began in 1996. This paper describes the details of reprocessing of ANWR seismic data for the current resource assessment.

During the current assessment, all of the seismic data acquired during 1984 and 1985 were reprocessed on SUN workstations using ProMAX processing software developed by Landmark, Inc. together with in-house developed software. All seismic data were stacked, migrated and depth-converted. Some seismic lines, which were acquired segmentally (at different times and using different sources) were merged into single lines. In addition to the amount of reprocessing, the major difference between the 1987 and 1998 reprocessing is that 1998 reprocessing produced migrated depth sections instead of unmigrated time sections.

DATA ACQUISITION

From January to April of 1984, GSI acquired 606.6 mi (982.7 km) of seismic reflection data using dynamite sources and 152.5 mi (247.1 km) using Vibroseis sources (Table SP1). During the second phase of data acquisition (1985), GSI obtained 692.3 mi (1121.5 km) seismic reflection data using Vibroseis source (Table SP1) (Foland and Lalla, 1987). Dynamite and Vibroseis recording parameters are listed in Table SP2. The major differences between the 1984 and 1985 seismic data are that (1) no dynamite data were recorded in 1985, (2) the sweep length was changed from 5 to 8 s in 1985, and (3) the correlated record time was changed from 8 to 6 s in 1985. Notice that the common midpoint (CMP) interval is 55 ft except for lines those marked by an * in Table SP1. The marked line CMP interval is 82.5 ft.

DATA PROCESSING

The processing flowchart is shown in Figure SP1.

Demultiplex.   The majority of the field tapes were demultiplexed during the 1987 assessment and archived in the SEG-Y format. Only a small number of field tapes were demultiplexed during this assessment. The field tapes were reformatted from SEG-B into SEG-Y format. Because of the problems associated with reading SEG-Y, 6250 bpi, 9-track tapes, some data were recovered from the sorted tapes stored in the DISCO internal format using an in-house developed program. The single most time-consuming and difficult problem encountered during this reprocessing was reading the SEG-Y tapes.

Geometry definition. The demultiplexed seismic data is in shot order. In order to process the data , it should be in CMP order. In order to sort seismic data into CMP order, we have to define the geometry of the field layout, including the source and geophone locations, group interval, station numbers, live stations and others (Table SP2). During this step, the elevations and uphole times or uphole depths were also stored in the database.

Gain, deconvolution and elevation statics. As mentioned in Leinbach and others (1987), when the dynamite source is detonated within the permafrost, the ice is fractured and continues to fracture, which creates secondary sources that are sometimes called "ice breaks". Some examples are shown in Leinbach and others (1987). These strong secondary sources often mask weak primary signals. An earlier study (Leinbach and others, 1987) indicates that surgical mute, which takes out the amplitude where the ice breaks are present, works adequately. Tests indicate that automatic gain control (AGC) is an alternative to the surgical mute, even though information about the relative amplitude is lost. Because our primary concerns in the reprocessing were prospect mapping and structural interpretation, preserving the relative amplitude was not considered important. Therefore using an AGC with a 300 ms window is acceptable.

In order to increase the temporal resolution, a two-window spiking deconvolution with operator lengths of 180 ms was applied to both the dynamite and Vibroseis data (minimum phase deconvolution for the dynamite data and zero phase for Vibroseis data). The design gates for the deconvolution were spatially varying, but other parameters were fixed.

Because the elevations of the seismic lines sometimes vary significantly (from the complexly deformed area to the undeformed coastal plain), a floating datum was chosen for the processing instead of a fixed flat datum. The floating datum was determined by smoothing the actual elevations (smoothing operator runs from 100 to 350 CMP's). Using this floating datum or normal moveout (NMO) datum, elevation statics were computed and applied to individual traces. This floating datum was corrected to a final flat datum (sea level) prior to migration.

Shot-domain F-K filtering. Coherent noise appears differently in different domains. An ice break appears as a secondary source in the shot-domain, and appears as a low velocity linear moveout event in the stacked section.

Other scattered noises including in-line and off-line sources appear differently in the shot, receiver or CMP domain (Tsai, 1984; Larner and others, 1983). Coherent noise can be suppressed somewhat after stack using two-dimensional (space and time) filtering, but the optimum way to suppress the coherent noise is the application of 2-dimensional filtering in the different domains before stack, where the coherent noise manifest itself differently from the signal.

Figure SP2a shows a stacked section without two-dimensional filtering and Figure SP2b shows the same stacked section with shot-domain two-dimensional filtering, which was applied in the frequency (F) and wavenumber (K) domain (F-K filtering). The majority of linear moveout events shown in Figure SP2a are caused by the ice breaks. These events mask the primary reflections in varying degrees. Figure SP2b indicates that the shot-domain F-K filtering suppresses these linear moveout events somewhat and improves the signal to noise ratio significantly throughout the section. However, there still remains a noticeable amount of linear moveout events with low apparent velocity in the section. These residual linear moveout events cannot be suppressed in the shot domain, because they are manifested in the receiver domain. Figure SP2c shows the stacked result with shot and receiver domain F-K filtering before stack. The same parameters of the F-K filtering were applied to both the shot- and receiver-domain. Figure SP2c indicates that most of the linear moveout events are suppressed after shot- and receiver-domain F-K filtering, but some signal strengths in the upper section (less than 1 s) are reduced relative to Figure SP2b.

During this reprocessing only shot-domain F-K filtering was applied. In certain parts of some profiles receiver-domain F-K filtering may be used as an option to improve the stack quality.

Velocity analysis and NMO correction. Standard velocity analyses were used to estimate the stacking velocity at 50 or 100 CMP intervals. An example is shown in Figure SP3. Figure SP3 has 4 display panels, which helps to estimate the stacking velocity accurately; they are from left to right semblance, gather, constant velocity stack, and interval velocity with maximum semblance panels. A correct stacking velocity is indicated by (1)a red colors (higher semblance) in the semblance panel, (2)horizontal reflections in the gather panel, (3) highest amplitude and focused events in the constant velocity panel, and (4) reasonable interval velocity values in the

interval velocity panel. The information supplied in theses panels help choose the optimum stacking velocities when conflicting events occur in the velocity analysis. For example, the semblance panel shows that the event near 3 s has higher semblance at the lower velocities than the picked velocities. However the lower stacking velocities would produce negative interval velocities. Although the interval velocity derived from stacking velocity has no physical meaning in some cases, interval velocity still guides the user in picking a reasonable stacking velocity.

The NMO corrections were applied using an automatic stretch mute with a maximum percentage of stretch of about 20%.

Residual statics. Surface consistent residual statics were computed using maximum power of CMP stacks. This method utilizes the fact that the stack power is maximum when the shot and receiver statics are optimally estimated and this method is effective in the low signal-to-noise data. Usually a 500 ms window with multiple gates and a pilot trace composed of 31 traces were used. This method worked remarkably well for the data shot in the coastal plain. But for some data acquired in the complexly deformed area it did not work as well, because a window to guide the static computation could not be picked.

The velocity analysis and residual static computation is an iterative process. Until a satisfactory stack section is obtained or there is no further significant changes in the stacking velocity, the process iterates as shown in Figure SP1. Usually a minimum of 2 iterations were adequate, but sometimes 3 iterations of static and velocity analysis were required.

Stack. The CMP gathers were stacked with the optimum velocities and statics. We tested a variety of stack methods using a median (instead of summing the samples, takes the median of the samples at each trace time), mean (sums the sample values and divides by a square root of the number of samples), and weighted mean (before summing, the samples are multiplied by weights; e.g., weights proportional to the offsets to reduce the multiple energy). The mean method usually worked effectively and in a couple of cases, a weighted or median method was used instead.

Shot-domain DMO. The stacking velocity or NMO velocity depends on the dip of the reflector. It is well known that the conventional stacking method cannot stack both a flat and dipping layer occurring simultaneously

because of the dip dependence of the stacking velocity. The dip moveout (DMO) process is a method to improve the stack quality by compensating for the dip effect in the NMO equation.

The arrival time for a single reflector is given by the following equation (Levin, 1971).

$$(1) \quad T^2(x) = T^2(0) + x^2 \cos^2(\;)/V^2 = T^2(0) + x^2/V_{nmo}^2$$

where T is the two-way travel time from a source to a receiver, x is an offset distance,   is a dip angle of a reflector, V is the medium velocity, and Vnmo is a normal moveout velocity or stacking velocity. In a multi-layered case, the right side of Equation (1) is approximately correct and the normal moveout velocity Vnmo becomes the root mean square velocity (Vrms). Because the stacking velocity (or Vnmo) analysis approximates the right side of Equation (1) with hyperbolas, Vnmo contains the dip effect.

To see the effect of dip and interval velocity on the moveout time, Equation (1) is changed into the following formula (Yilmaz, 1987).

$$(2) \quad T^2(x) = T^2(0) + x^2/V^2 - x^2 \sin^2(\;)/V^2$$

In this equation , the first part of moveout (the second term, x^2/V^2) is called zero-dip normal moveout and the second part (the third term) is associated with dip moveout (DMO). DMO processing is a scheme to compensate for the dip dependence of the NMO equation and make the NMO equation independent of the dip angle. One advantage of DMO processing is the improvement of velocity analysis, as it provides velocities which are more appropriate for use in migration (Deregowski and Rocca, 1981). Most of the data has been processed using DMO in the shot-domain except for a few lines in the undeformed area.

As indicated in the flow chart, the velocity and the statics for the regular stack process were the inputs to the DMO processing. DMO velocities were estimated using the same method as mentioned above. An example of a DMO velocity analysis is shown in Figure SP4. This analysis uses the same range of CMP gathers as that used in Figure SP3. Careful examination of Figure SP4 shows that the DMO velocities in Figure SP4 are

slightly slower than those in the regular velocity analysis shown in Figure SP3. This is expected because the dip dependence of the velocity has been compensated for in the DMO velocity analysis.

We carefully compared the DMO stack and regular stacked sections. Although the DMO velocities were more appropriate to the subsequent migration velocity analysis, the DMO stacked sections were usually inferior to the normal stacked sections in the overall signal-to-noise ratio and in mapping shallow dipping events. Therefore, the majority of final depth sections were derived from the stacked data processed without using DMO.

Post-stack deconvolution. Because of the different sources used (dynamite and Vibrosies) and the reverberatory energy present in the stacked section, a post-stack deconvolution was applied to all stacked data in order to correct for the differences in source type and increase temporal resolution. A 1000 ms AGC was applied before the post-stack deconvolution, which included a second-zero crossing and wavelet deconvolution. Second-zero crossing deconvolution is a type of predictive deconvolution where the prediction distance is the second-zero crossing of the auto-correlation of the trace. A single window with an 180 ms operator length was used.

In wavelet processing, a variable norm deconvolution method by Gray (1979) was applied in the reprocessing. About 200 random windows (window length is about 16 ms for the dynamite data and about 20 ms for the Vibroseis data) were selected between about 200 and 1000 ms in the stacked data and wavelets were estimated using different norms, window lengths, and design area. The deconvolved outputs were compared visually and optimum parameters were chosen, even thought this process is subjective and based on experience. A single deconvolution operator was derived from the optimum parameters and applied to the whole line.

Figure SP5 shows an example of this post-stack process. Figure SP5a shows the final stacked section without the post-stack deconvolution and Figure SP5b shows the result after the post-stack deconvolution was applied. One advantage to the post-stack deconvolution is in it's ability to effectively merge two or three different lines, because this post-stack processing adequately compensated for the differences in the frequency content and phase of the wavelet present in different lines.

An example of the final stacked section is shown in Figure SP6.

Datum Correction and Filtering. To migrate the stacked data, they were corrected to a final flat datum (sea level) by using simple static shifts instead of the more accurate method based on the wave equation. Datuming based on the wave equation was not used in our processing sequence, but should be considered in future reprocessing. A band pass filter with 8-10-68-92 Hz pass band was also applied.

Migration. The stacked data were migrated using Stolt's wave-number frequency domain migration method using migration velocity models derived from the DMO stacking velocities, which will be described in detail in the section entitled " Derivation of Velocities". An example of a migrated section is given in Figure SP7, which is the migrated result of the data shown in Figure SP6.

Depth Conversion. The migrated data were depth-converted using average velocities (See Derivation of Velocities). Usually for the depth conversion, well data or vertical seismic profile (VSP) data are used to constrain the average velocity. Because no wells are located in the ANWR area, the average velocities are strictly derived from the DMO velocities. Depth sections were examined and if there were questions concerning the validity of depth section, the velocities were modified and the stacked data were migrated again with a new velocity model and depth-converted until an acceptable section was obtained.

As can be seen from the derivation of the average velocities, the converted depth sections contain many uncertainties due to the lack of well or VSP data, but the depth sections are geologically sound and grossly accurate. Therefore, these depth sections provide an additional advantage for structural interpretation and prospect mapping. An example is shown in Figure SP8, which is a time-to-depth converted section of Figure SP7.

Section Enhancement.   The small size figures such as those shown in Figures SP6, SP7, and SP 8 and the sections presented in the CD are plotted at 100- 200 traces /inch (horizontal scale) and 1 inch / second or 1 inch / 5000 ft (vertical scale). When the original stacked or depth sections are plotted at this small size, the section becomes difficult to interpret or the major reflections are obscured. This is apparent in the figures shown in the 1987 assessment (Bird and Magoon, 1987). To circumvent this problem, the seismic sections are enhanced to increase the visibility of major events

at the expense of detail. To enhance the visibility of seismic reflections the data were band pass filtered with 8-12-56-68 Hz pass band, were applied by a median filter using 3 by 3 grid and the amplitudes were modulated by the trace envelope as explained in Lee and others (1988).

DERIVATON OF VELOCITIES

Migration Velocity. Accurate interval or RMS velocity, which is smooth spatially and temporally, is required to migrate seismic data with minimum migration artifacts. Usually migration requires a velocity model. This velocity model is iteratively modified until a migrated output is geologically sound and the effect of processing artifacts such as migration smiles are minimized. Building a migration velocity model is not a simple matter, particularly in complexly deformed areas such as the southern part of ANWR.

Stacking velocity, which is optimum for the stack, is not optimum for the migration in many cases. Migrated sections using the stacking velocities frequently show over-migration, because the stacking velocity is usually higher than the RMS velocity owing to the effect of dip as shown in Equation (1) and ray-path dependence of the stacking velocity. In order to overcome this problem, migration velocity analysis is performed. A sound and popular method for migration velocity analysis is to migrate the seismic section with constant velocities and build a velocity model from the migrated output until the output is geologically sound.

Our procedure to do migration velocity analysis is as follows.
1) Estimate accurate RMS velocities from the DMO processed seismic data. As mentioned previously, the DMO velocity is close to the RMS velocity of the subsurface because the effect of dip on the velocity is removed or reduced.
2) As mentioned earlier, the processing datum is a floating datum. This is the reference point of the DMO velocity. To do migration, a velocity model with a flat datum is required. Therefore, the picked DMO velocity is shifted in time to the final flat datum. In this case the flat datum is sea level. An example of the DMO velocity with flat datum correction is shown in Figure SP9.
3) Tests indicate that the DMO velocity is high for the migration. In order to perform a better migration the DMO velocities were altered systematically by reducing velocity as the time increases.

At zero time 100% of picked DMO velocity is used, at the level of the top of the Pre-Mississippian (TPM), the velocity is reduced to 95 % , and at about 1-2 s below the TPM, the velocity is reduced to 90 % of the picked DMO velocity. Since the TPM is spatially varying, the velocity modulation is spatially variant.

4) As indicated in Figure SP9, the picked DMO velocity is not smooth enough to migrate the stacked data adequately. Therefore the velocities were smoothed using triangular tapers in time and space. We used 300 CMP as the half height of a triangular smoother in space and 500 ms as the half height of a triangular smoother in time. The velocity model from Figure SP9 with all modification and smoothing is shown in Figure SP10.

5) We performed the migration with the velocity derived in stage 4 and examined the output. Based on the migrated output, the migration velocity was modified to image the subsurface as accurately as possible. Except for a few cases, the velocity model built at the stage 4 proved adequate for migration and subsequent processing.   The migrated section shown in Figure SP7 is the output using the velocity model shown in Figure SP10 to the section shown in Figure SP6.

Average velocity. To convert a migrated time section to a depth section, an average velocity model or an interval velocity model is required. We used the final migration velocity model derived in stage 5 as the input to the average velocity model in time. To derive average velocities, a method using smooth gradient function was used. This method offers the ability to output a smoothly varying interval velocity function containing no sudden changes in the rate at which the velocity field is changing. The depth section shown in Figure SP8 is the result of the application of the average velocity model derived from the migration velocity model shown in Figure SP10.

Average velocity to TPM. The average velocity derived in the above section is independently derived without considering the crossing lines. At the tie points between two lines, the average velocities usually differ slightly because the smoothing procedure is done in two dimensions instead of three dimensions and there may be some anisotropy. This implies that the depth sections may not tie perfectly between lines. To tie the depth sections together, a three-dimensional smoothing procedure is necessary. This was not available to us at the time of reprocessing.

Smoothed average velocity tables were derived for seismic lines where a strong TPM (top of the Pre-Mississippian metasedimentary rocks) reflection event was observed. The tables gave the average velocity to time horizons in 250 msec increments. The reflection time of the TPM for each velocity analysis was derived from a 1:100,000 scale time contour map, and the average velocity value from the table was interpolated and plotted on the TPM time contour map. Over 600 average velocity values were plotted and evaluated. Discrepancies at line crossings were generally less than 200 ft/sec in the unreformed zone, but frequently exceeded 500 ft/sec in the deformed area (i.e., southern and eastern part of 1002).

At the beginning of this process, we thought that the average velocity map could be simplified into 15 to 20 control points which could be entered into the GEOGRAPHIX GIS work station and then contoured into a smooth average velocity map for conversion of the time map to a depth map, which was required for prospect evaluation. However, after more than ten iterations of these velocity maps, 92 control points were selected to represent the complex lateral velocity gradients within the 1002 area of ANWR (Figure SP11). This map indicates that the average velocity to the TPM ranges from less than 9,800 ft/sec in the northwest edge of 1002 to more than 16,000 ft/sec in southeastern 1002. Therefore, this study area has more than a 60 % lateral change for the average velocity to the TPM. Additional second order variations were clearly defined over many of the mapped structural highs and basins.

At this time, the USGS does not have a software package to automatically interpolate and smooth all of the average velocity analyses generated in the ANWR seismic reprocessing (>1500) into a three-dimensional model. Such software could certainly improve the second order anomalies in the velocity model, particularly in the deformed zone.

DISCUSSION

The focus of this reprocessing effort has been on the generation of the migrated depth-section for prospect mapping and structural and stratigraphic interpretation. Therefore, developing a three-dimensional interval or average velocity model is one of the most important aspects. Unfortunately , as mentioned previously, an efficient software to derive a smooth three-dimensional velocity models for multiple horizons was not

available to us. Therefore, only one three-dimensional velocity model, for the TPM horizon, was feasible in the current study. Consequently, crossing lines which tie in time do not necessary tie in the depth sections. Figure SP12 shows depth sections that cross each other. Depths tie fairly well above 5000 ft, but there is about a 400 ft depth difference between the strong event near 5500 ft. In a sense, the discrepancy of the depths between two crossing lines can be used to determine the accuracy of the depth section. On average, the difference is less than 5%.

 Another way of estimating the accuracy of depth sections can be accomplished by comparing the seismically derived depth to the well log depth. For example, the projected TPM depth from the West Staines State 2 well is within 2 % of the depth estimated from the depth section, which is more typical of the accuracy in the undeformed part of 1002.

One problem in using velocity smoothing is the significant distortion at the edge of the lines caused by the extrapolation of the velocity field. Where possible (see Table SP1), we merged and migrated shorter lines into one continuous profile to reduce not only the migration edge effect but also the migration velocity edge effect.

The optimum way to derive a depth section is to use pre-stack depth migration. When we started this project in 1996, the reprocessing was performed on a SUN SPARCStation 2. This work station was too slow to test pre-stack depth migration. In August 1997, this system was upgraded to a SUN ULTRA 1, which is fast enough to run some testing of pre-stack depth migration. Figure SP13a shows a depth section derived using the flow chart shown in Figure SP1 and Figure SP13b shows the result of pre-stack depth migration. The input for the pre-stack depth migration were the interval velocity in depth derived from the final migration velocity model and final residual statics. The result shown in Figure SP13b is the result of one-pass finite difference shot domain pre-stack depth migration. Further iterations of migration velocity analysis may provide an even better image than the one shown in this figure. However this illustrates the advantages of pre-stack depth migration. As shown in this figure pre-stack depth migration provides a more focused image and improved signal-to noise ratio, particularly at about 10,000ft in the right side of the section. One problem of the post-stack migration used in this reprocessing is it's inability to image under a complex structure, because the post-stack time migration cannot correctly handle ray bending. The unfocused images on the right

side of Figure SP13a are imaged better in the pre-stack depth migrated section.

SUMMARY AND CONCLUSION

The major accomplishments of reprocessing the seismic data for the 1998 resource assessment are:

1) Post-stack processing including wavelet deconvolution provided significantly improved temporal resolution. Wavelet processing produced consistent wavelets which in turn improved the quality of the merged seismic data.

2) By merging appropriate lines, the edge effects of the migration and velocity field were significantly reduced and increased the overall seismic data quality.

3) Depth sections, in addition to final stack and migrated time sections, helped in the structural and stratigraphic interpretations and the mapping the prospects.

ACKNOWLWDGEMENTS

REFERENCES

Bird, Kenneth J. and Magoon, Leslie B., eds., 1987, Petroleum geology of the northern part of the Arctic National Wildlife Refuge, northeastern Alaska: U.S. Geological Survey Bulletin 1778, 329 p.

Clough, N.K., Patton, P.C., and Christiansen, A. C. , eds., 1987, ArcticNational Wildlife Refuge, Alaska, coastal plain resource assessment-Report and recommendations to the Congress of the United States andfinal legislative environmental impact statement: Washington D.C., U.S.Fish and Wildlife Service, U.S. Geological

Survey, and Bureau of LandManagement, v. 1 (Report)-208 p., v.2 (Appendix - Public comments andresponses)-998 p.

Deregowski, S. and Rocca, F., 1981, Geometrical optics and wave theory forconstant-offset sections in layered media, Geophysical Prospecting, v. 29, p. 374-3.

Foland, Richard L. and Lalla, Douglas J., 1987, Seismic-reflection data acquisition, processing, and interpretation *in* Bird , Kenneth J. and Magoon, Leslie B., eds., Petroleum geology of the northern part of the Arctic National Wildlife Refuge, northeastern Alaska: U.S. Geological Survey Bulletin 1778, p. 235-243.

Gray, W.C., 1979, Variable norm deconvolution: Palo Alto, CA, StanfordUniversity Ph.D. Thesis, p.101.

Larner, K., Chambers, R., Yang, M., Lynn, W., and Vai, W., 1983, Coherent noise in marine seismic data: Geophysics, v. 48, p. 884-886.

Lee, M.W., Agena, W.F., and Hutchinson, D.R., 1988, Processing of the GLIMPCE multichannel seismic data: U.S. Geological Survey Open FileReport 88-225, 46 p.

Leinbach W. James, Miller, John, J., and Lee, Myung W., 1987, Seismic-reflection data processing *in* Bird , Kenneth J. and Magoon, Leslie B., eds., Petroleum geology of the northern part of the Arctic National Wildlife Refuge, northeastern Alaska: U.S. Geological Survey Bulletin 1778, p. 225-233.

Levin, F.K, 1971, Apparent velocity from dipping interface reflections: Geophysics, v. 36, p. 510-516.

Tsai, C. J., 1984, An analysis leading to the reduction of scattered noise on deep marine seismic records: Geophysics, v. 49, p. 17-26.

Yilmaz, Ozdogan, 1987, Seismic data processing: Society of Exploration of Geophysics- Investigations in Geophysics, V.2, , 526 p.

Table SP-1. Reflection Seismic lines on and adjacent to the Arctic National Wildlife Refuge
[*, Shot with 165 ft Station Intervals; ** , Trademark of Continental Oil Company]

1984				1985	
Dynamite		Vibroseis**		Vibroseis**	
AN84-1	Merged with ANV84-1	ANV84-1	Merged with AN84-1	AN85-1	
AN84-2		ANV84-3	Not Converted (Overlap)	AN85-2	Merged with AN85-2A
AN84-3A	Merged with AN84-3, AN84-3B	ANV84-7		AN85-2A	Merged with AN85-2
AN84-3	Merged with AN84-3A, AN84-3B	ANV84-8		AN85-3	
AN84-3B	Merged with AN84-3A, AN84-3	ANV84-10	Merged with AN84-10, AN85-16	AN85-7	
AN84-4		ANV84-12	Merged with AN84-12	AN85-8	Merged with AN84-6
AN84-5		ANV84-14	Merged with AN84-14	AN85-10	
AN84-6	Merged with AN85-8	ANV84-15		AN85-14	
AN84-7*		ANV84-16	Merged with AN84-16	AN85-15	
AN84-8		ANV84-17		AN85-16	Merged with AN84-10, ANV84-10
AN84-10	Merged with ANV84-10, AN85-16	ANV84-18	Merged with AN84-18, AN85-48	AN85-17	
AN84-11*	Merged with AN84-13	ANV84-19		AN85-18	
AN84-12	Merged with ANV84-12	ANV84-30	Merged with AN84-30	AN85-19	
AN84-13*	Merged with AN84-11	ANV84-32	Merged with AN84-32, AN85-52	AN85-20	
AN84-14	Merged with ANV84-14	ANV84-34		AN85-21	
AN84-16	Merged with ANV84-16	ANV84-34A		AN85-22	
AN84-18	Merged with ANV84-18, AN85-48	ANV84-34B		AN85-24	
AN84-20		ANV84-36		AN85-25	
AN84-22	Merged with AN85-30, AN85-32	ANV84-38		AN85-25A	
AN84-24		ANV84-40		AN85-26	
AN84-26		ANV84-48		AN85-28	
AN84-28		ANV84-50		AN85-30	Merged with AN84-22, AN85-32
AN84-30	Merged with ANV84-30	ANV84-52		AN85-32	Merged with AN84-22, AN85-30
AN84-32	Merged with ANV84-32, AN85-52	ANV84-56		AN85-34	
AN84-34		ANV84-58		AN85-36	
		ANV84-60		AN85-38	
				AN85-42	
				AN85-44	
				AN85-46	
				AN85-48	Merged with AN84-18, ANV84-18
				AN85-50	
				AN85-52	Merged with AN84-32, ANV84-32

Table SP-2 Parameters of seismic data acquisition in the ANWR area
[*, 330-ft shot and 165-ft group interval; **, 61 percent and ***, 39 percent of the 1985 data; n.c., no change; n.a., not applicable]

Parameter	Dynamite Source	Vibroseis Source	
Year Recorded	1984	1984	1985
Charge size	60 lb	n.a.	n.a.
Shot Depth	75 ft	n.a.	n.a.
Shot Interval	220 ft	n.a.	n.a.
	330 ft	n.a.	n.a.
Vibrator Interval	n.a.	110 ft	110 ft
Sweep Length	n.a.	5 s	8 s
Vibrators/Sweep	n.a.	4 or 5	4 or 5
Sweeps/VP	n.a.	8 or 6	12 or 8
Sweep Spectrum	n.a.	10-80 Hz	8-90 Hz
Group Interval	110 ft, 165 ft	110 ft	110 ft
Groups	120	120	120
Geophone Array	Linear, 24 geophones per group	n.c.	n.c.
Source Array	Point	160/164 ft	220 ft
Spread Geometry	2805-275-0-275-10725 (ft)	2805-275-0-275-1075 (ft)	3025-495-0-495-10945 (ft)**
	10065-330-0-330-10065 (ft)*		2915-385-0-385-10835 (ft)***
Fold	30	60	60
Recorder	Texas Instruments DFS-V	n.c.	n.c.
Sample Rate	2 ms	4 ms	4 ms
Record Length	8 s	13 s	14 s
Geophones	GSC 20D, 10-Hz Resonance	n.c.	n.c.
High-cut Filter	128-Hz, 72-dB/Octave Cutoff	n.c.	n.c.
Low-cut Filter	8-Hz, 18-dB/Octave Cutoff	n.c.	n.c.
Miles Recorded	606.6	152.5	692.3

Figure SP1: Seismic data processing flow
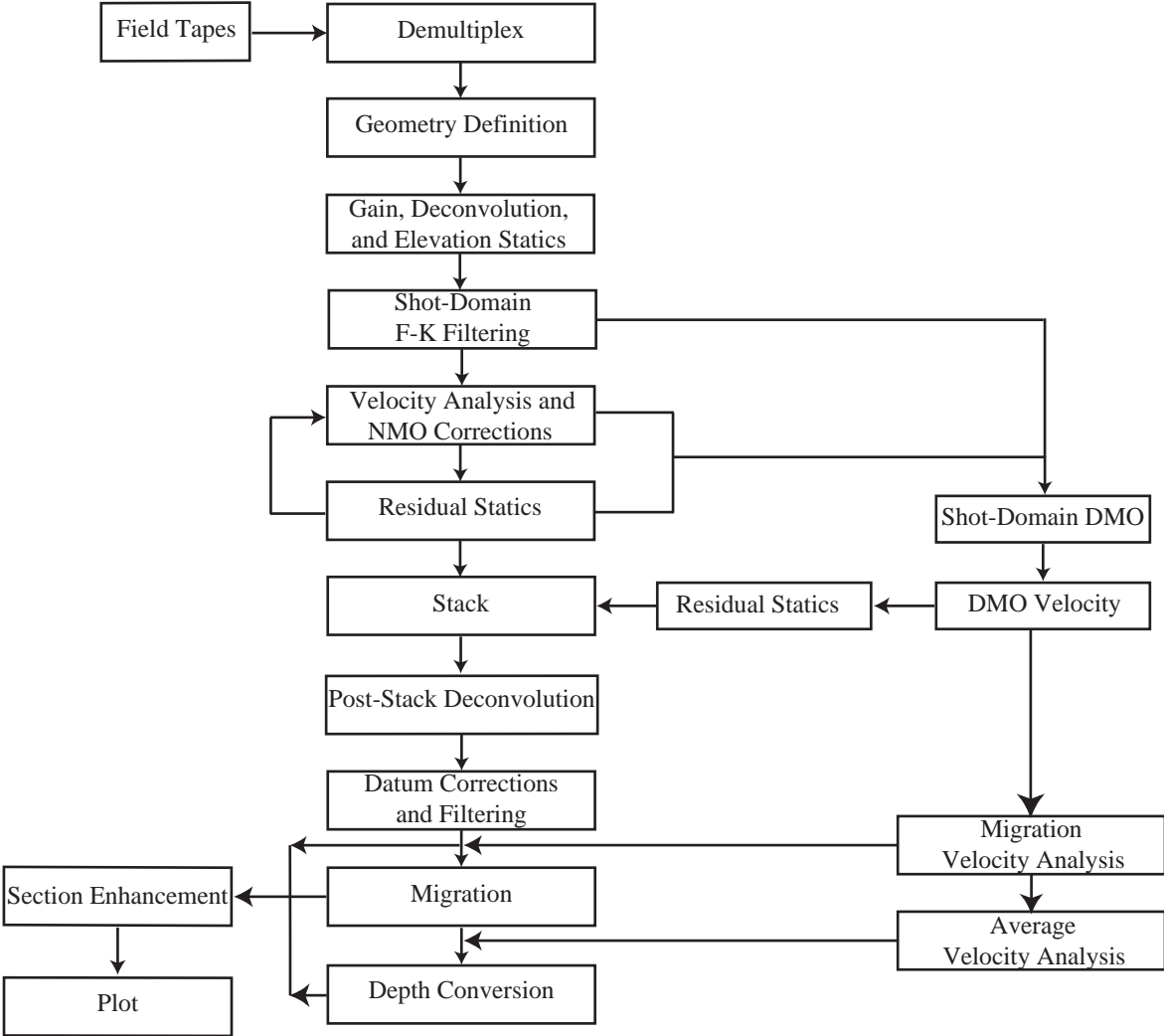
Figure SP2 : An example of stacked seismic data showing the effect of pre-stack two-dimensional filtering:
   a) No filtering applied.
   b) Shot-domain frequency-wavenumber (FK) filtering applied.
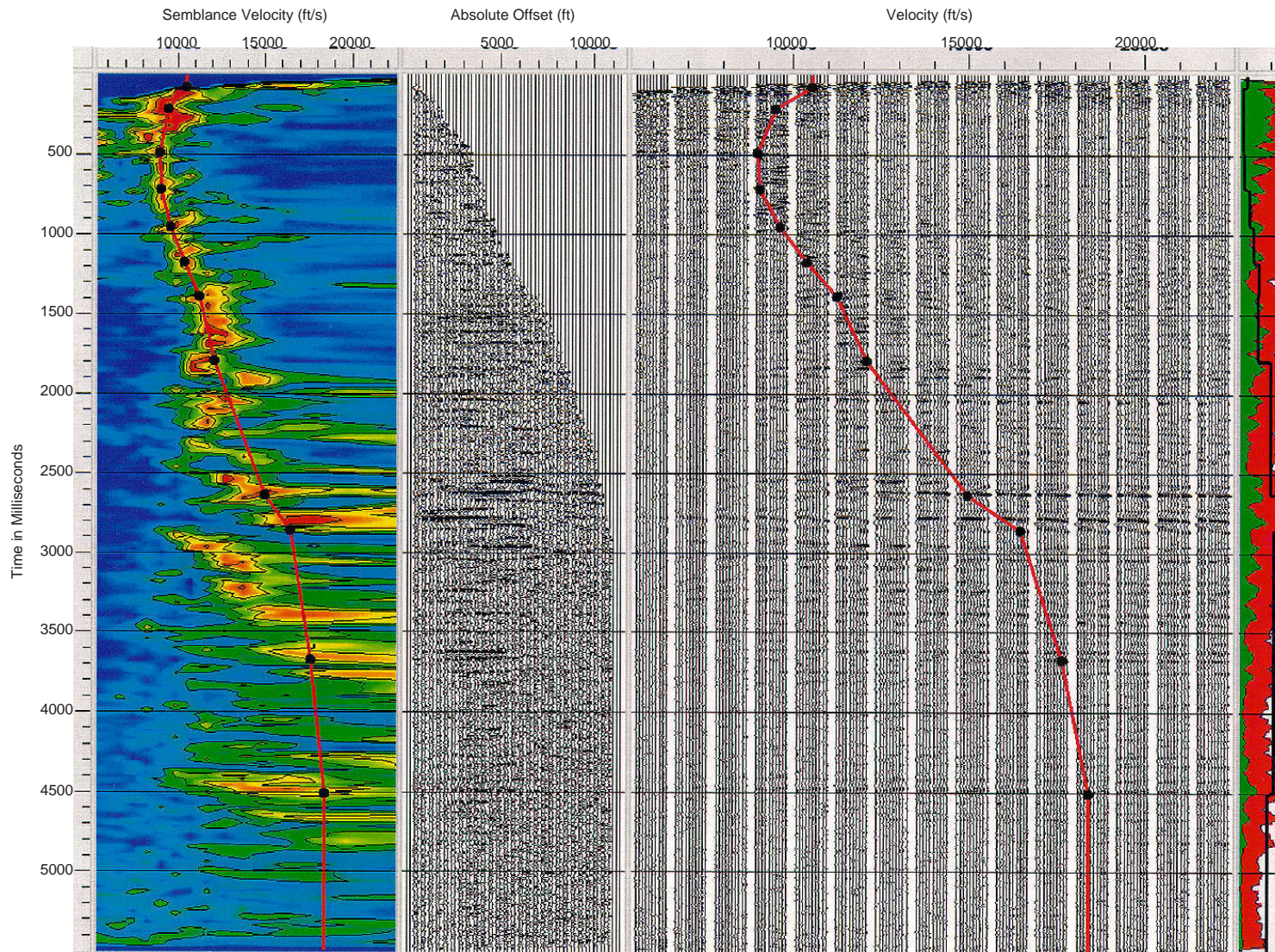   c) Shot- and receiver-domain FK filtering applied.
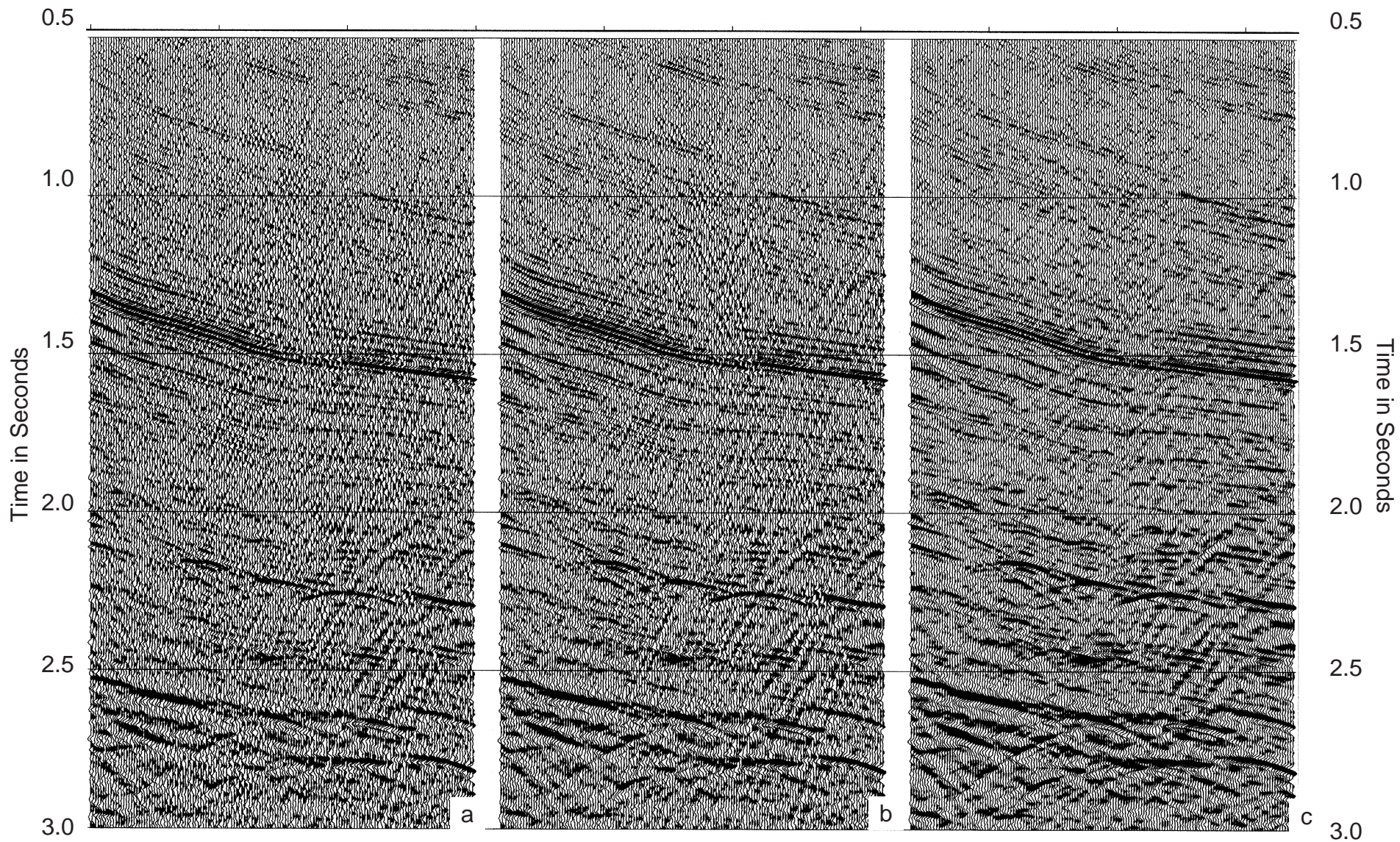
Figure SP3 : An example of velocity analysis without a dip moveout (DMO) correction. From left to right, Semblance velocity panel, CMP gather panel, constant velocity stack panel, Interval velocity (black line) and semblance (color) panel.

Figure SP4: An example of velocity analysis with a dip moveout (DMO) correction. From left to right, Semblance velocity panel, CMP gather correction, constant velocity stack panel, Interval velocity (black line) and semblance (color) panel.
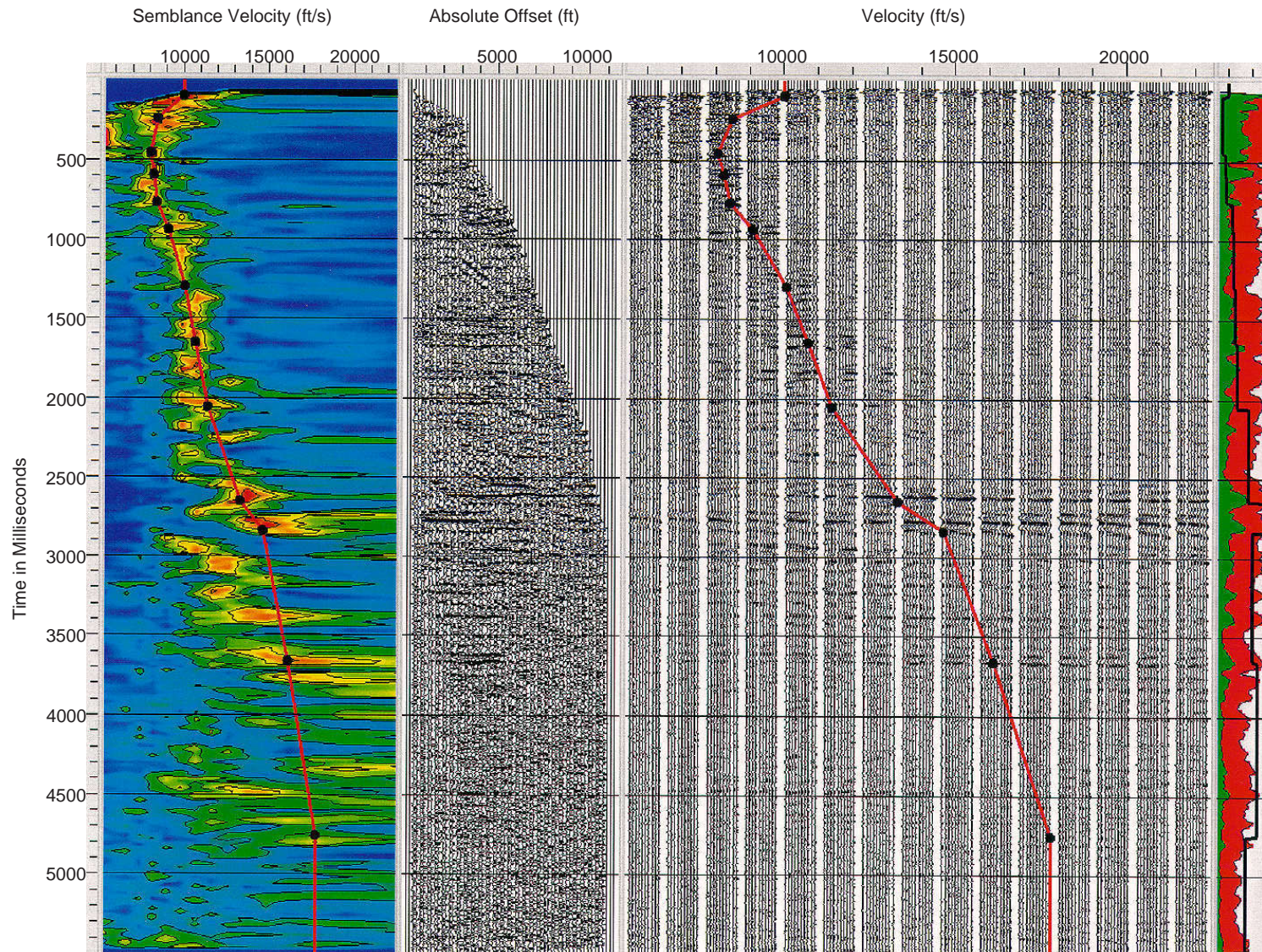
Figure SP5: An example showing the effect of post-stack deconvolution
        a) Without post-stack deconvolution
        b) With post-stack deconvolution (Second-zero crossing
            predictive deconvolution and wavelet deconvolution)
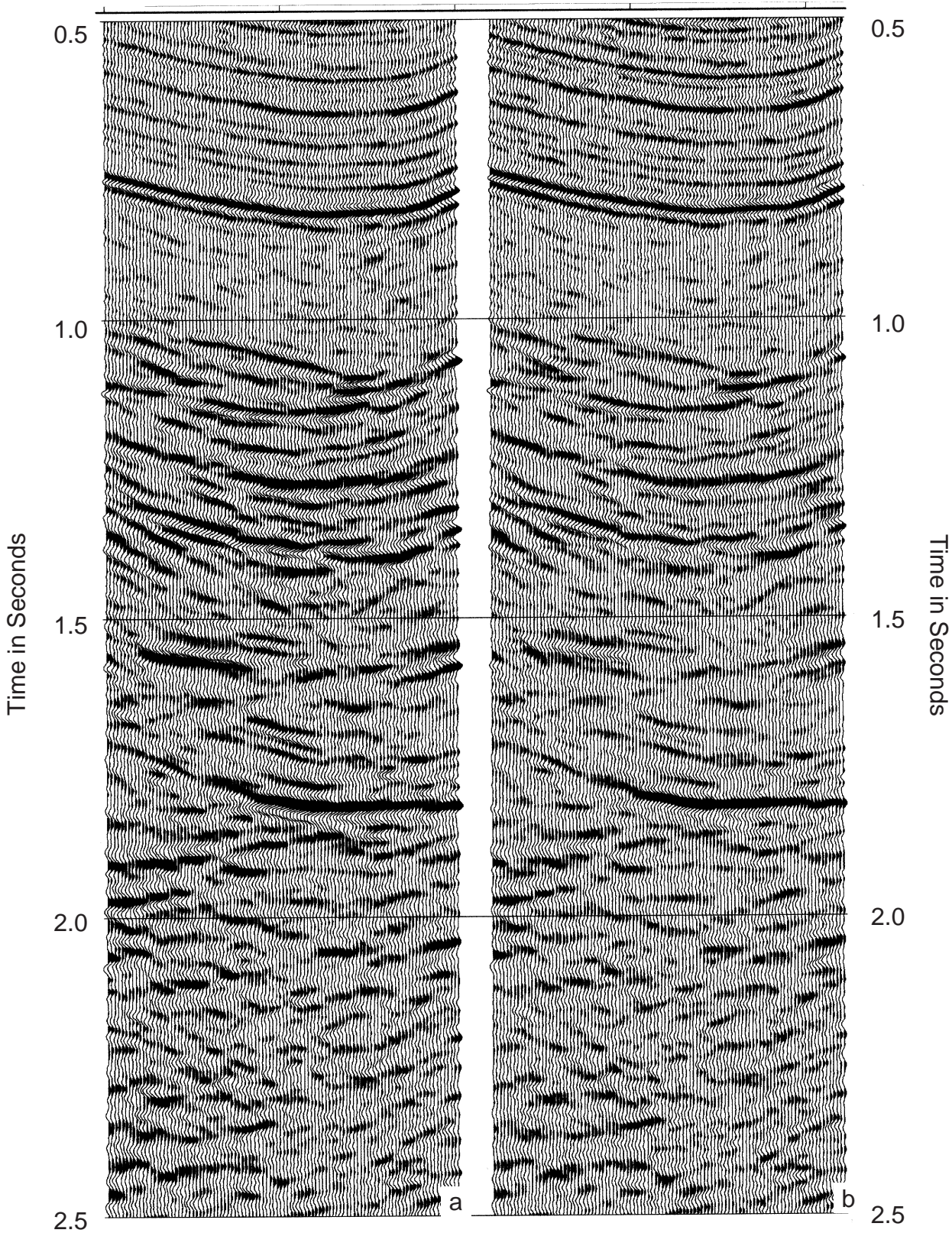
Figure SP6: An example of a stacked (unmigrated) section without DMO correction. TPM indicates the top of Pre-Mississippian.

TPM

Time in Seconds

5 Miles
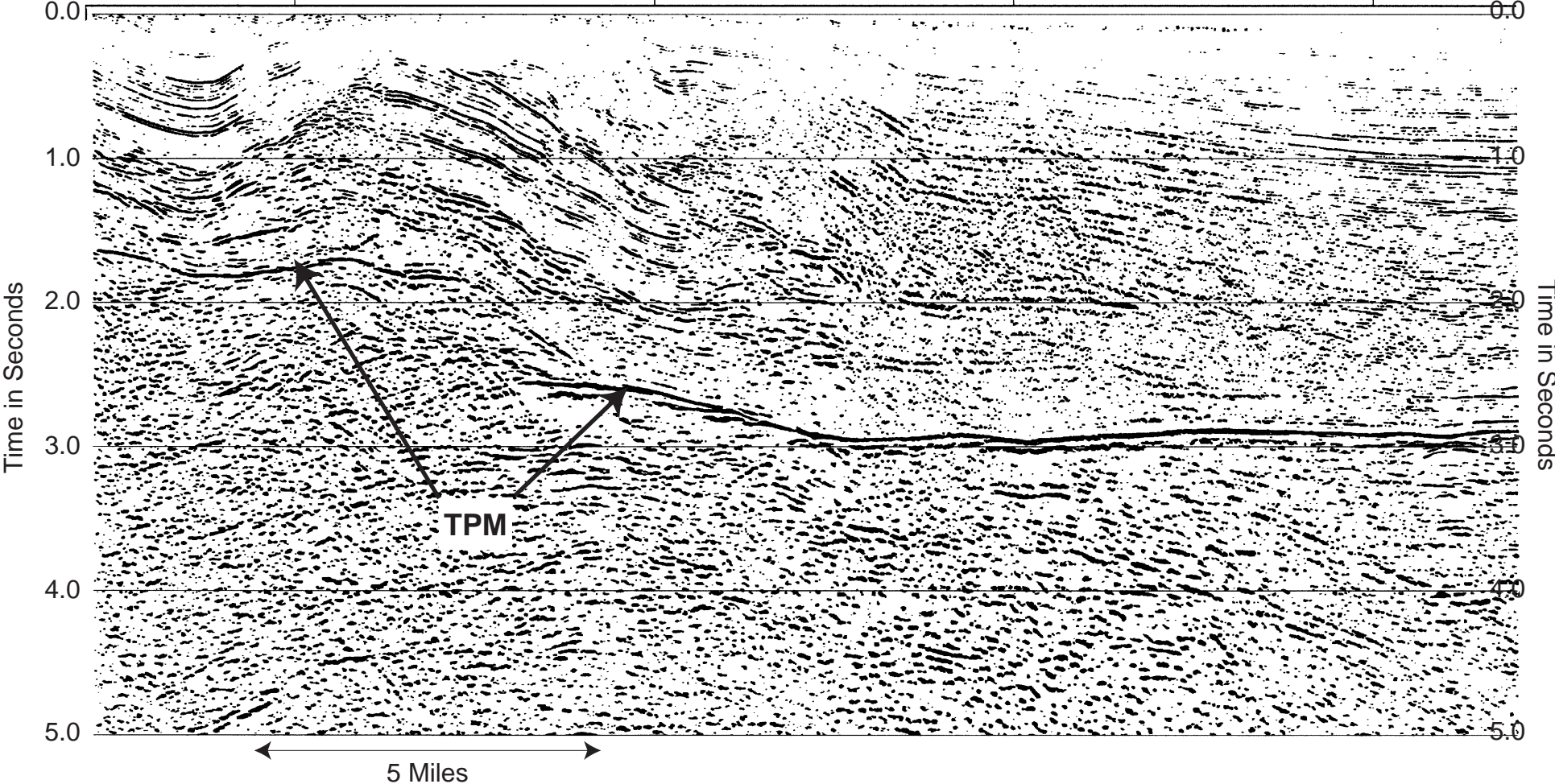
Figure SP7: Migration of data shown in Figure SP6 (data without DMO correction). Velocities used for migration were from data which had a DMO correction, and smoothing (Figure SP10). TPM indicates the top of Pre-Mississippian.
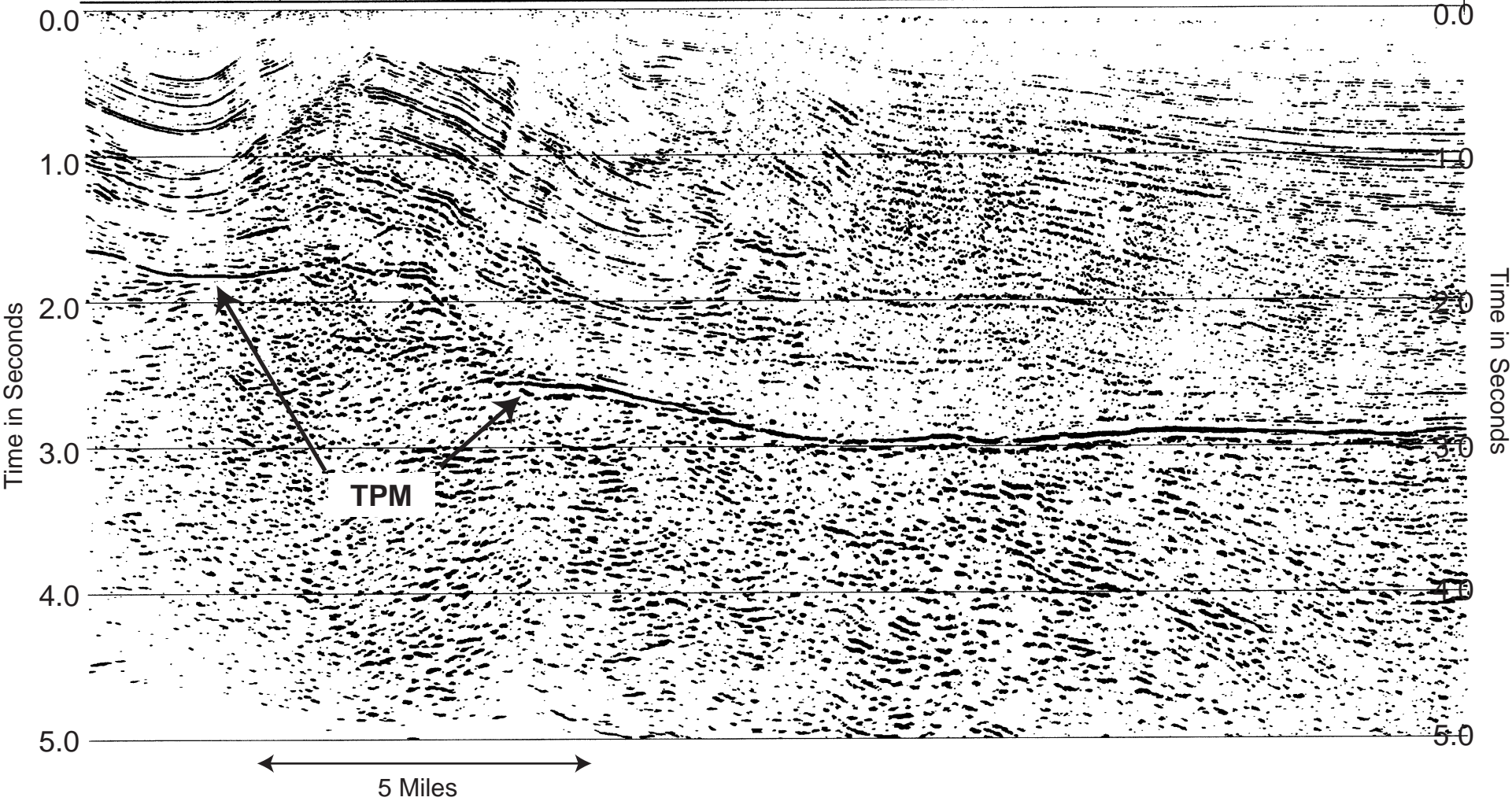
Figure SP8: An example of a depth-converted section of the time section shown in Figure SP7. TPM indicates the top of Pre-Mississippian.
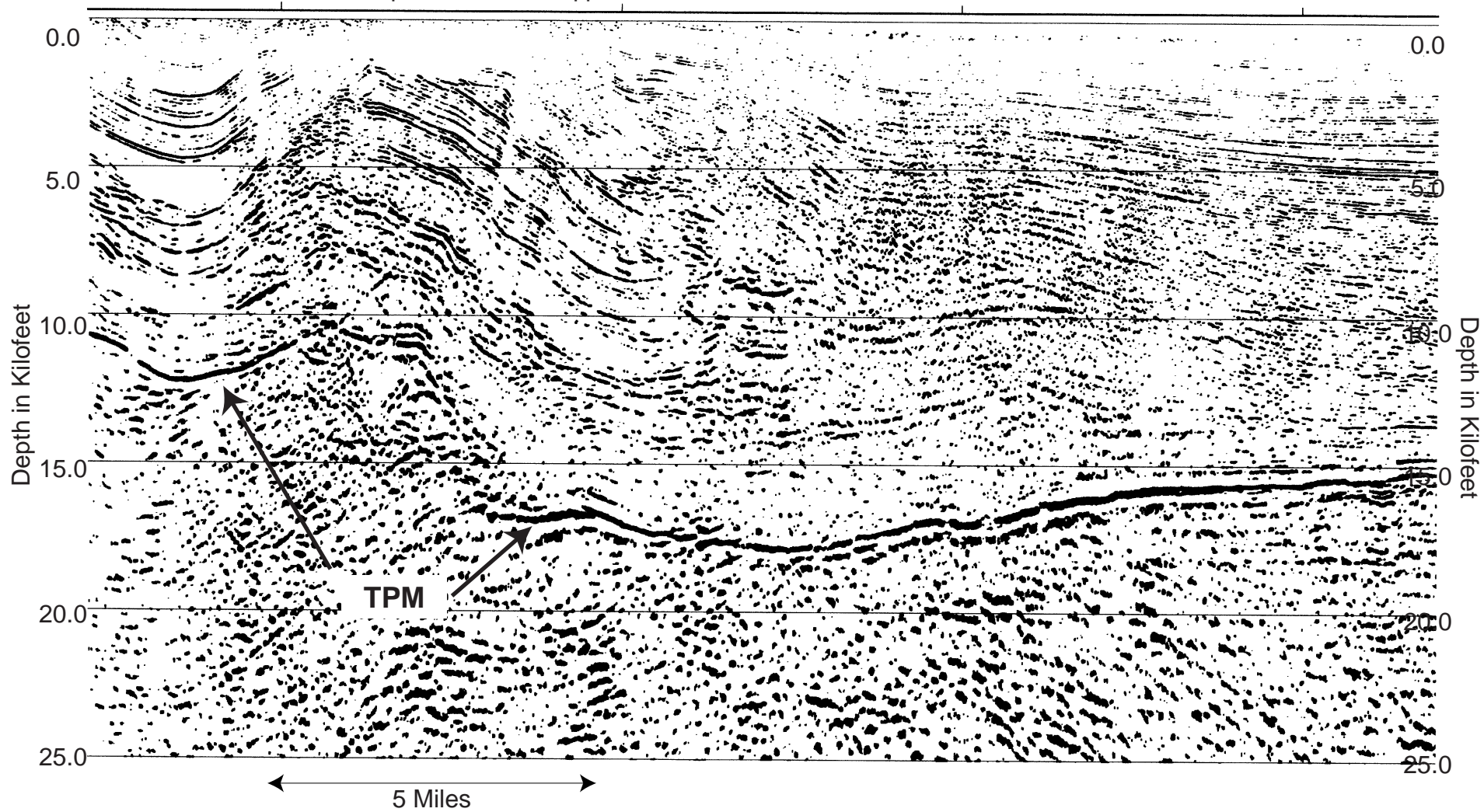
Figure SP9: Stacking velocities with DMO correction, shifted from a floating datum (smoothed surface elevations) to a flat datum (sea level)
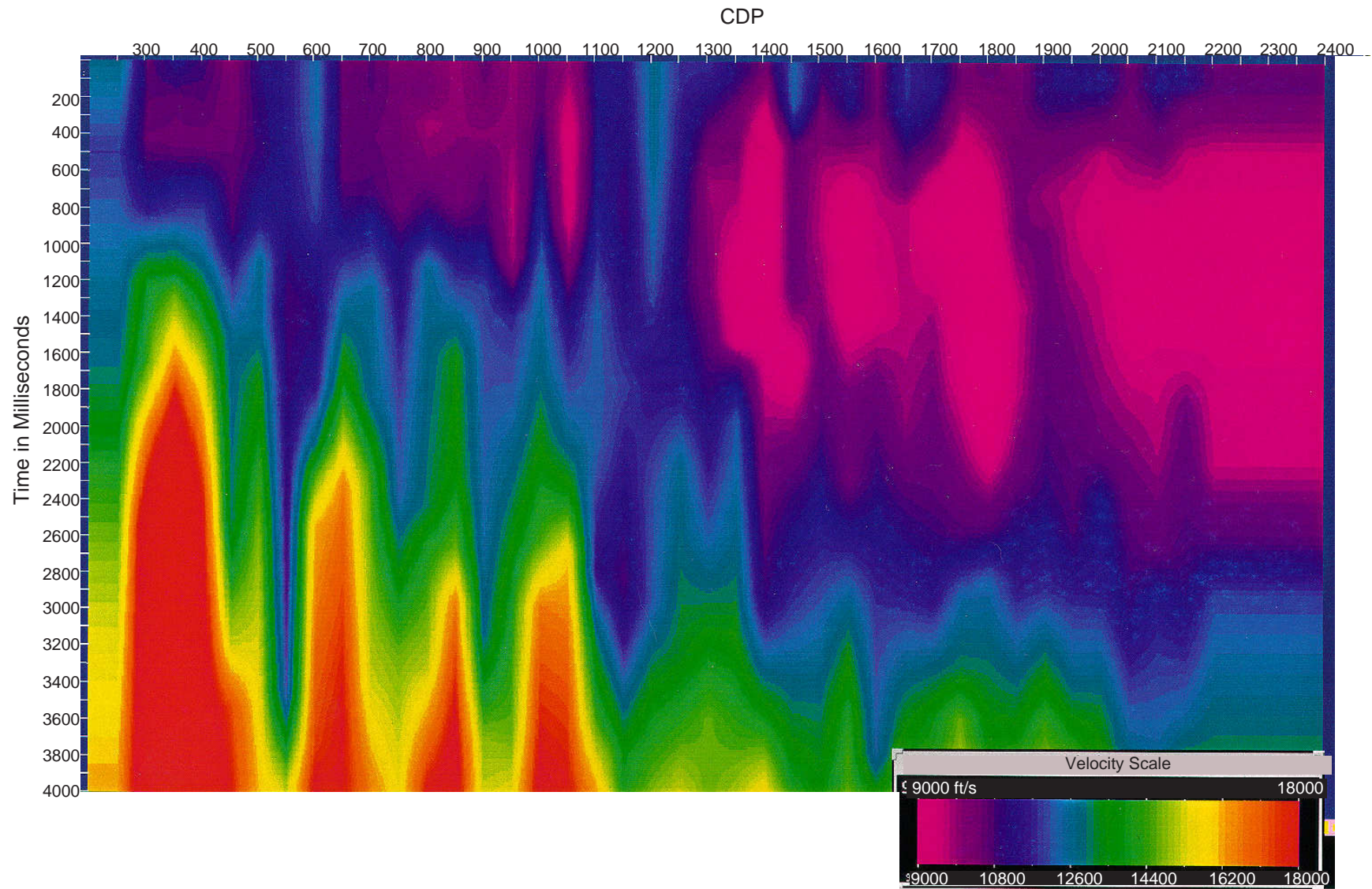
Figure SP10: Migration velocities derived from the stacking velocities shown in Figure SP9 with two-dimensional smoothing and modification. These velocities were used to migrate ths stacked section shown in Figure SP6.
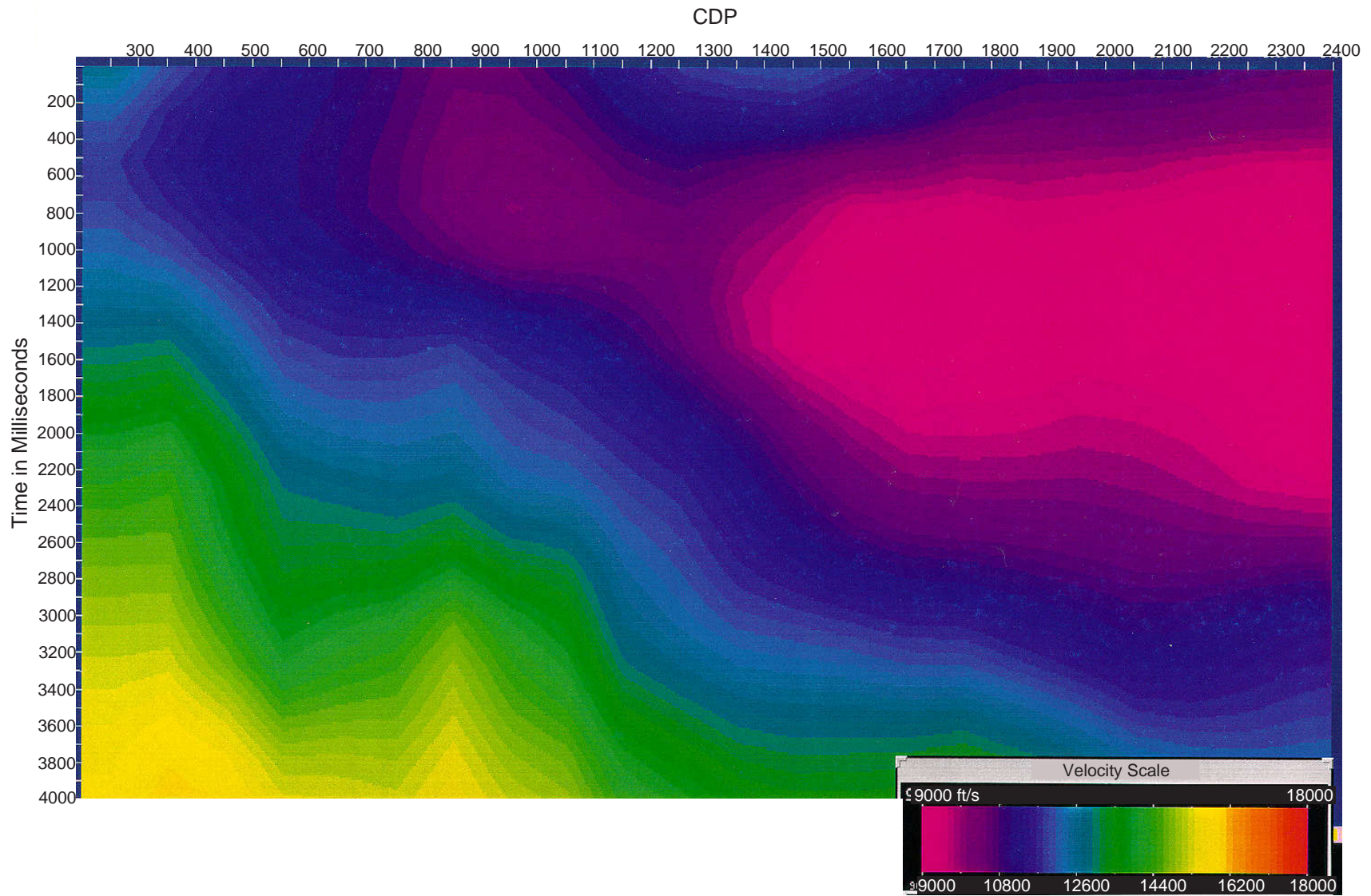
Figure SP11. Average velocity model to the top of the Mississippian (TPM) derived from migration velocity model. This velocity model was used to map the prospects for the undeformed Franklinain, deformed Franklinian, and the Niguanak-Aurora plays
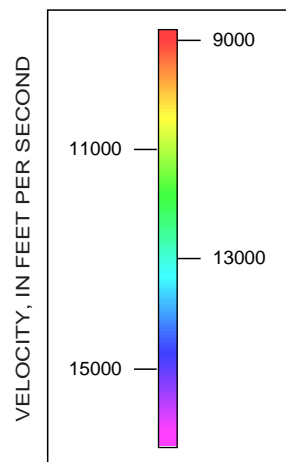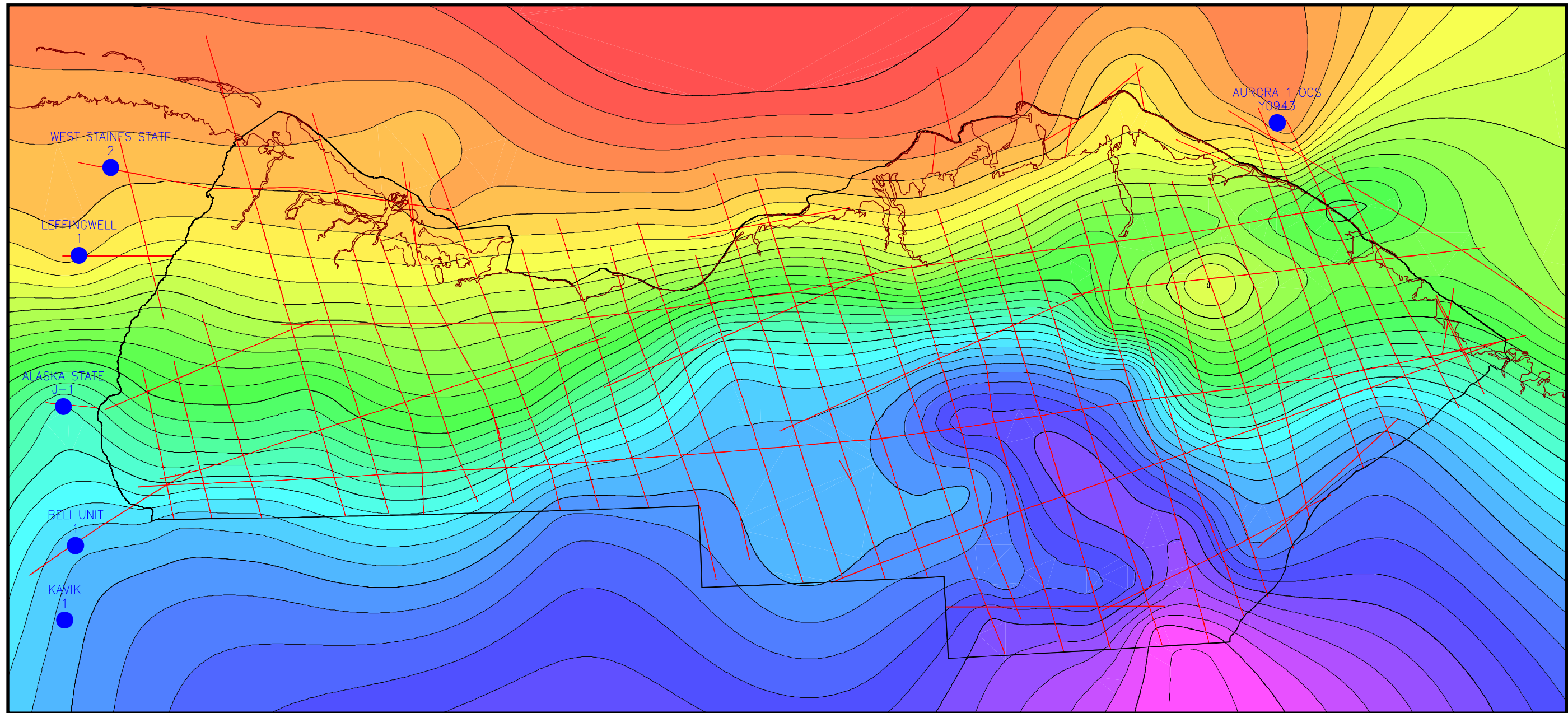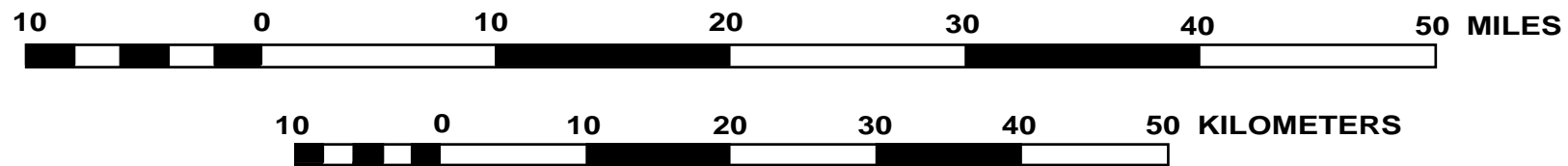
Figure SP12: An example showing the problems associated with depth conversion.
a) Post-stack time migration and depth conversion of a strike line.
b) Post-stack time migration and depth conversion of a dip line.
Notice about 400 ft difference between the two plots for the strong events near 5500 ft in depth.
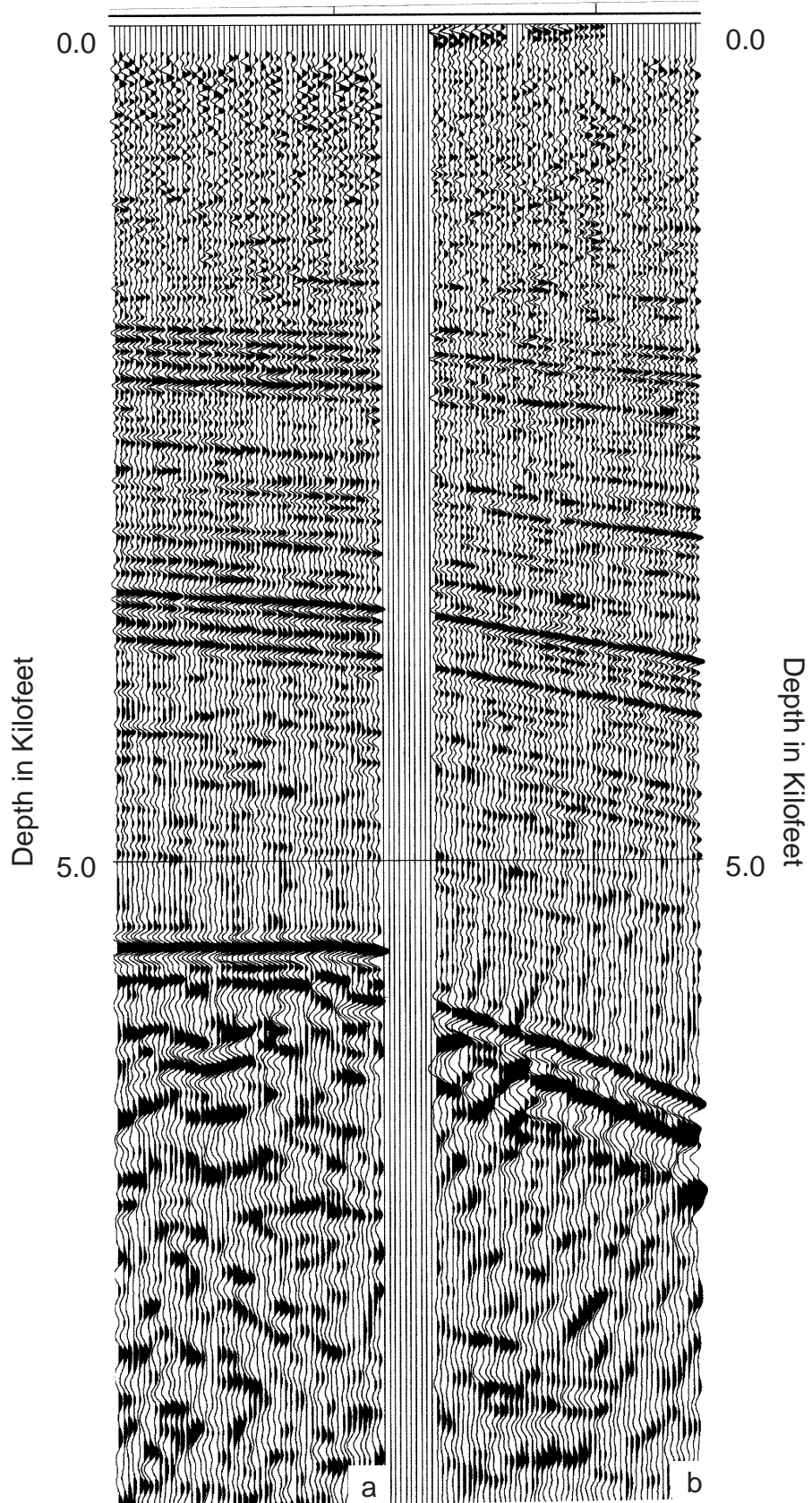
Figure SP13: Comparison of post-stack depth conversion and pre-stack depth migration
      a) Post-stack time migration and depth conversion using an average velocity model
      b) Pre-stack depth migration using a finite difference algorithm in the shot-domain